Computer Physics Communications 185 (2014) 1515–1528

Contents lists available at ScienceDirect

Computer Physics Communications

journal homepage: www.elsevier.com/locate/cpc

Time-splitting pseudo-spectral domain decomposition method for the soliton solutions of the one- and multi-dimensional nonlinear Schrödinger equations

Ameneh Taleei, Mehdi Dehghan *

Department of Applied Mathematics, Faculty of Mathematics and Computer Science, Amirkabir University of Technology, No. 424, Hafez Ave., 15914, Tehran, Iran

ARTICLE INFO

Article history:
Received 13 December 2012
Received in revised form
22 November 2013
Accepted 23 January 2014
Available online 31 January 2014

Keywords:
Nonlinear Schrödinger (NLS) equation
Pseudo-spectral (PS) method
Operator splitting method
Overlapping multi-domain technique
Multi-dimensional nonlinear Schrödinger equation
Alternating direction implicit (ADI) technique
Domain decomposition

ABSTRACT

In this paper, we study the simulation of nonlinear Schrödinger equation in one, two and three dimensions. The proposed method is based on a time-splitting method that decomposes the original problem into two parts, a linear equation and a nonlinear equation. The linear equation in one dimension is approximated with the Chebyshev pseudo-spectral collocation method in space variable and the Crank–Nicolson method in time; while the nonlinear equation with constant coefficients can be solved exactly. As the goal of the present paper is to study the nonlinear Schrödinger equation in the large finite domain, we propose a domain decomposition method. In comparison with the single-domain, the multi-domain methods can produce a sparse differentiation matrix with fewer memory space and less computations. In this study, we choose an overlapping multi-domain scheme. By applying the alternating direction implicit technique, we extend this efficient method to solve the nonlinear Schrödinger equation both in two and three dimensions, while for the solution at each time step, it only needs to solve a sequence of linear partial differential equations in one dimension, respectively. Several examples for one- and multi-dimensional nonlinear Schrödinger equations are presented to demonstrate high accuracy and capability of the proposed method. Some numerical experiments are reported which show that this scheme preserves the conservation laws of charge and energy.

1. Introduction

1.1. Solitons in optical fibers

The term soliton was introduced in the 1960s, but the scientific research of solitons had already started in the 19th century when John Scott-Russell observed a large solitary water-wave in a canal near Edinburgh. A very significant contribution to the experimental and theoretical studies of solitons was the identification of various forms of robust solitary waves in nonlinear optics [1]. Optical solitons may be naturally subdivided into three broad categories: temporal, spatial, and spatiotemporal ones. They may exist in the form of one-dimensional or multi-dimensional objects [2]. One-dimensional temporal solitons in optical fibers with a cubic nonlinearity were predicted by Hasegawa and Tappert [3], and observed experimentally by Mollenauer et al. [4] while stable self-trapping of light in the spatial domain was first observed in planar waveguides by Maneuf et al. [5]. Spatial two-dimensional solitary waves were first observed in photorefractive crystals, which feature a saturable nonlinearity [6], and in optical media with a quadratic nonlinearity [7]. Nonlinear optical effects are capable to create waveguiding channels by solitary waves that make spatial optical solitons attractive candidates for adaptive concepts of waveguiding in telecommunication and information processing applications. Nonlinear optics allow the unique possibility to combine the basic features of nonlinear effects with definite applications in information technology [8]. The interested reader can see [9] for some applications of the Schrödinger equation.

1.2. Nonlinear Schrödinger equation with soliton solutions

Nowadays, many equations of nonlinear phenomena are known to possess soliton solutions that have been identified in a large variety of wave and particle systems in nature [10,11]. The nonlinear Schrödinger equation in its many versions is one of the

* Corresponding author. Tel.: +98 21 64542503.
E-mail addresses: ataleei@aut.ac.ir (A. Taleei), mdehghan@aut.ac.ir, mdehghan.aut@gmail.com (M. Dehghan).

http://dx.doi.org/10.1016/j.cpc.2014.01.013
0010-4655/

most important models of mathematical physics with applications to different fields such as nonlinear optics [12,6,3,4], water-wave [13], plasma physics [14], electromagnetic wave propagation in nonlinear materials [15] and many other fields [10,16]. The effective dynamics of solitary waves [17] for nonlinear Schrödinger equations with external potential [18–21] or without external potential [6,3,8,4] have been the object of numerous studies in the last twenty years. Regarding the importance for the nonlinear Schrödinger equation, numerous numerical methods have been employed (see [22–28] and the references inside). Recently, Zhu et al. [28] developed symplectic and multi-symplectic wavelet collocation methods to solve the linear and nonlinear Schrödinger equations in two dimensions. Bratsos [22] presented a numerical scheme based on the use of rational approximations in a two-time level recurrence relation to solve the nonlinear Schrödinger equation in 1D. Kong et al. [29] studied a six-order compact alternative direction implicit (ADI) finite difference method for multi-dimensional Schrödinger equation. Gao and Xie [24] applied alternating direction implicit compact finite difference schemes for the numerical solution of two-dimensional Schrödinger equation.

In the present paper, we consider the nonlinear Schrödinger equation

$$i\frac{\partial}{\partial t}\psi + \alpha\Delta\psi + w\psi + \beta|\psi|^2\psi = 0,$$
$$\mathbf{x} \in \Omega \subset \mathbb{R}^d,\ d = 1, 2, 3,\ t > 0, \tag{1.1}$$

where $i^2 = -1$ and the complex wave function $\psi(\mathbf{x}, t)$ may represent a probability amplitude, the amplitude of an electric field or the velocity field of a fluid. Also the external potential function $w(\mathbf{x}, t)$ is a bounded real function and α, β are real constants.

It is well known that the nonlinear Schrödinger equation has an infinite number of conservation laws. It is easy to prove the following invariants under the assumption of homogeneous or periodic condition:

$$Q(t) = \int_{\mathbb{R}^d} |\psi(\mathbf{x}, t)|^2 d\mathbf{x} = Q(0), \quad t > 0, \tag{1.2}$$

and when the potential function w is independent of t (i.e., $w(\mathbf{x}, t) \equiv w(\mathbf{x})$) then

$$E(t) = \int_{\mathbb{R}^d} \left[\alpha|\nabla\psi(\mathrm{X}, t)|^2 - w(\mathbf{x})|\psi(\mathbf{x}, t)|^2 - \frac{\beta}{2}|\psi(\mathbf{x}, t)|^4\right] d\mathbf{x}$$
$$= E(0), \quad t > 0, \tag{1.3}$$

where the above two conservation laws are corresponding to the conservation of charge and energy, respectively.

It is worth to point out that the soliton solution of the wave propagation problems in a very large or unbounded domain for the nonlinear Schrödinger equation is an interesting and important problem in applications [30,31]. Therefore, the stable and accurate numerical methods are required in the large computational domain. In one dimension, several schemes have been proposed for the soliton solution of nonlinear Schrödinger equation (see [32,23,33,26] and the references inside). For the nonlinear Schrödinger equation in higher dimensions, numerous computational methods have been investigated [34,24,29,35] but the numerical studies in large domains, especially for the nonlinear Schrödinger equation with non-periodic boundary conditions, have been paid less attention [27,36,28]. Also we refer the interested reader to [37–40] for alternative approaches proposed for finding the numerical solution of Schrödinger equations.

1.3. The aim of the current paper

It has been shown that spectral methods can provide a very useful tool for the solution of time-dependent partial differential equations because of their spectral accuracy, when the geometry of the problem is smooth and regular [41]. The Fourier pseudo-spectral time-splitting (FPTS) method is one of the spectral methods which is applied for various nonlinear Schrödinger equations by many authors such as Weideman and Herbst [42], Muruganandam and Adhikari [43], and Bao et al. [44]. But this method is very efficient for the nonlinear Schrödinger equation with periodic boundary conditions because it is based on Fourier approximation in space. For the problems with non-periodic boundary conditions, Jacobi polynomials such as Chebyshev, Legendre, Laguerre, and Hermite are recommended [41,45]. In this paper, a Chebyshev pseudo-spectral method is proposed for the solution of the nonlinear Schrödinger equation in one, two and three dimensions in large domain with non-periodic boundary conditions.

In this work we also use the Strang splitting scheme [46]. The operator splitting methods have shown many advantages, especially for some difficult problems. Most natural splitting schemes are frequently constructed according to either physical components and subsystems, such as density, velocity, energy and pressure, or physical processes, such as reaction, diffusion and convection, or dimension, such as in the alternating direction implicit (ADI) method. The basic idea in the split step methods is to decompose the original problem into subproblems which are simpler than the original problem and then to compose the approximate solution of the original problem by using the exact or approximate solutions of the subproblems in a given sequential order [47–50].

Considering the Strang splitting scheme for Eq. (1.1) in one dimension, we will split it into a nonlinear part and a linear part. The solution of the nonlinear part with the time-independent potential function can be solved exactly and for the linear part we propose the Chebyshev pseudo-spectral collocation method for the space discretization and the Crank–Nicolson scheme for the time discretization. The Crank–Nicolson scheme is one of the implicit finite difference schemes that is unconditionally stable for the Schrödinger equation [51]. The proposed method is easily generalized to two and three dimensions by using ADI technique, while for the solution at each time step, it only needs to solve a sequence of linear systems in one dimension.

The spectral methods [52–54] are global in nature, which means that they approximate a function and its derivatives at a point by using the information at all points in the domain. Thus the matrices that comprise the discrete system in pseudo-spectral method are full matrices. The goal of this paper is to study numerical solution of Eq. (1.1) in the large space domain. In order to achieve high approximation accuracy, the number of spatial grid points must be large enough. The use of large number of points leads to the pseudo-spectral differentiation matrices that in the single-domain pseudo-spectral method are large and full, and have large memory requirements and expensive computations, correspondingly.

The multi-domain pseudo-spectral method has some merits compared with the single-domain method. It can reduce memory requirements because it leads to sparse matrices that yields huge saving in memory structure especially in large domain with large grid points. It also allows for the best use of parallel computers and more flexibility in computations.

The multi-domain pseudo-spectral methods have been widely used for many years. For example, in [55–57] the Chebyshev pseudo-spectral multi-domain method investigated for the Navier–Stokes equations. Kuria and Raad [58] proposed an implicit multi-domain Chebyshev spectral collocation technique for solving advection–diffusion Burgers equation and Reynolds equation.

Pfeiffer et al. [59] demonstrated two versions of pseudo-spectral collocation technique with domain decomposition for coupled nonlinear elliptic PDEs; touching and overlapping subdomains. For the time discretization of nonlinear partial differential equations, unlike the implicit methods such as Crank–Nicolson that usually need to solve a system of nonlinear equations at each time step, explicit schemes such as Runge–Kutta methods are generally easier to be implemented but they are conditionally stable. The multi-domain pseudo-spectral method with explicit Runge–Kutta method for the time integration is investigated for some nonlinear equations such as the Fisher equation [60], the soliton solution of coupled nonlinear Schrödinger equations [33] in one dimension. It was shown that the use of multi-domain pseudo-spectral method leads to a significant relaxation of the restricting stability condition, allowing the use of much larger time steps. However, these explicit schemes will require much smaller time steps for the stiff equations such as nonlinear Schrödinger equation in multi-dimensional space. In this paper, we are going to study a multi-domain pseudo-spectral scheme by using time splitting and ADI scheme for the nonlinear Schrödinger equation with particular attention to high dimensions in spatial large domain. The proposed scheme is very efficient and attractive because of unconditional stability in time and easy implementation for the numerical solution of nonlinear Schrödinger equation in one and multi-dimensional spaces without solving the nonlinear system at each time step.

1.4. The organization of the current paper

The rest of this paper is organized as follows: In Section 2 we demonstrate the time splitting pseudo-spectral domain decomposition method and implement it for the nonlinear Schrödinger equation in one and three dimensions. Using the expression of the algorithm, we show that the proposed method is straightforward. We apply our approach on several examples in Section 3. The results of numerical experiments are compared with analytical solution for confirming the good accuracy of the proposed scheme and investigating the conserved quantities charge and energy. In Section 4 the conclusion of this paper is presented.

2. Numerical scheme

In this section we demonstrate the multi-domain pseudo-spectral method with the Strang splitting scheme for the NLS equation (1.1) in one and three dimensions.

2.1. The Strang splitting scheme

The operator splitting schemes for the nonlinear equation $U_t = (\mathcal{L} + \mathcal{N}(U))U$ can be done to decompose this problem into linear and nonlinear subproblems at each time step. In this paper, we choose the second-order Strang splitting scheme for decomposition of the linear subproblem $U_t = \mathcal{L}U$ and the nonlinear subproblem $U_t = \mathcal{N}(U)U$ as follows

$$U(\mathbf{x}, t+\tau) = \exp\left(\frac{\tau}{2}\mathcal{N}\right)\exp(\tau\mathcal{L})\exp\left(\frac{\tau}{2}\mathcal{N}\right)U(\mathbf{x}, t) + O(\tau^3). \tag{2.1}$$

Therefore, for solving Eq. (2.1), from time $t = t_n$ to time $t = t_{n+1}$, we will have the following sequence of updating

$$U^* = \exp\left(\frac{\tau}{2}\mathcal{N}(U^n)\right)U^n, \tag{2.2}$$

$$U^{**} = \exp(\tau\mathcal{L})U^*, \tag{2.3}$$

$$U^{n+1} = \exp\left(\frac{\tau}{2}\mathcal{N}(U^{**})\right)U^{**}, \tag{2.4}$$

where $U^n = U(\mathbf{x}, t_n)$, $U^{n+1} = U(\mathbf{x}, t_{n+1})$ and $\tau = t_{n+1} - t_n$. Note that the high-order operator splitting schemes can be constructed to reduce the splitting errors in the Strang formulae (see [61]).

In Eq. (1.1) the linear part

$$\psi_t = i\alpha\Delta\psi, \tag{2.5}$$

in one dimension will be solved by the Crank–Nicolson method in time and multi-domain pseudo-spectral (MDPS) method in space. The nonlinear part

$$\psi_t = iw\psi + i\beta|\psi|^2\psi, \tag{2.6}$$

with the time-independent potential function $w(\mathbf{x})$ can be integrated exactly in the physical space. In some cases, this subproblem with the time-dependent potential function $w(\mathbf{x}, t)$ cannot be integrated easily. We use the midpoint rule as follows

$$\int_{t_n}^{t_{n+1}} w(\mathbf{x}, t)dt = \tau w\left(\mathbf{x}, \frac{t_n + t_{n+1}}{2}\right) + O(\tau^3). \tag{2.7}$$

Note that we choose the Crank–Nicolson method in time discretization for linear subproblem and the midpoint rule for numerical integration in nonlinear subproblem which have the same order of accuracy with the Strang splitting scheme considered in this study.

2.2. The MDPS method for the linear dispersion equation

Consider the linear dispersion equation

$$\frac{\partial\psi}{\partial t} = i\alpha\frac{\partial^2\psi}{\partial\xi^2}, \quad \xi \in \Omega = [\xi_L, \xi_R], t > 0, \tag{2.8}$$

with the initial condition

$$\psi(\xi, 0) = \psi^0(\xi), \tag{2.9}$$

and the boundary conditions

$$\psi(\xi_L, t) = f_1(t), \qquad \psi(\xi_R, t) = f_2(t). \tag{2.10}$$

First we discretize the time variable in Eq. (2.8) with the Crank–Nicolson method. Therefore we will have

$$\frac{\psi^{n+1} - \psi^n}{\tau} = \frac{i\alpha}{2}(\psi^{n+1}_{\xi\xi} + \psi^n_{\xi\xi}), \tag{2.11}$$

where $\psi^n = \psi(\xi, t_n)$, $\psi^{n+1} = \psi(\xi, t_{n+1})$ and $t_{n+1} = t_n + \tau$.

Using the substitution of $u + iv$, u and v are real functions, instead of the complex function ψ in Eq. (2.11) we will have the following system

$$\begin{cases} u^{n+1} + \delta v^{n+1}_{\xi\xi} = u^n - \delta v^n_{\xi\xi}, \\ v^{n+1} - \delta u^{n+1}_{\xi\xi} = v^n + \delta u^n_{\xi\xi}, \end{cases} \tag{2.12}$$

where $\delta = \frac{\alpha\tau}{2}$. Now we approximate system (2.12) in the space variable with the overlapping MDPS method. In this method, without loss of generality, we consider a uniform partition consisting of M elements $\Omega^\mu = [\xi_L^\mu, \xi_R^\mu]$ with the same length $\ell = \frac{\xi_R - \xi_L}{M+(1-M)(1-\cos(\pi/N))/2}$ and $N+1$ grid points in each element, where the first two quadrature points of the element $\Omega^{\mu+1}$ coincide with the last two points of the element Ω^μ, i.e., $\Omega = \bigcup_{\mu=1}^M \Omega^\mu = \bigcup_{\mu=1}^M [\xi_0^\mu, \xi_N^\mu]$, $\xi_0^1 = \xi_L$, $\xi_N^M = \xi_R$, $\xi_{N-1}^\mu = \xi_0^{\mu+1}$, $\xi_N^\mu = \xi_1^{\mu+1}$. We choose the Chebyshev–Gauss–Lobatto (CGL) quadrature points, $\eta_j = \cos(\frac{N-j}{N}\pi)$; $j = 0, 1, \ldots, N$, in each element. In element Ω^μ, we will have

$$\begin{cases} u^{\mu,n+1} + \delta v^{\mu,n+1}_{\xi\xi} = u^{\mu,n} - \delta v^{\mu,n}_{\xi\xi}, \\ v^{\mu,n+1} - \delta u^{\mu,n+1}_{\xi\xi} = v^{\mu,n} + \delta u^{\mu,n}_{\xi\xi}, \end{cases} \tag{2.13}$$

where u^μ and v^μ are the solution over the μth element. Using the grid point values in one element, we can expand the function in that element and evaluate its derivatives. Now we introduce the operator of interpolation $u^{(\mu)}(\eta^\mu, t)$ and $v^{(\mu)}(\eta^\mu, t)$ on $\eta^\mu \in [-1, 1]$ in the form

$$\begin{cases} u^\mu(\eta^\mu, t) \simeq \sum_{j=0}^{N} \tilde{u}_j^\mu(t)\phi_j^\mu(\eta^\mu) = \Phi^\mu{}_{[0:N]}\hat{\mathbf{u}}^\mu, \\ v^\mu(\eta^\mu, t) \simeq \sum_{j=0}^{N} \tilde{v}_j^\mu(t)\phi_j^\mu(\eta^\mu) = \Phi^\mu{}_{[0:N]}\hat{\mathbf{v}}^\mu, \end{cases} \tag{2.14}$$

$$\Phi^\mu{}_{[0:N]} = [\phi_0^\mu(\eta^\mu), \ldots, \phi_N^\mu(\eta^\mu)],$$
$$\hat{\mathbf{u}}^\mu = [\tilde{u}_0^\mu(t), \ldots, \tilde{u}_N^\mu(t)]^T, \qquad \hat{\mathbf{v}}^\mu = [\tilde{v}_0^\mu(t), \ldots, \tilde{v}_N^\mu(t)]^T,$$

where the basic functions $\phi_j^\mu(\eta^\mu)$ are the Lagrangian interpolation in the CGL points. In order to use the above approximation, on the arbitrary interval $[\xi_L^\mu, \xi_R^\mu]$, we can use the mapping

$$\eta^\mu : [\xi_L^\mu, \xi_R^\mu] \longrightarrow [-1, 1],$$
$$\eta^\mu(\xi^\mu) = \frac{2}{\xi_R^\mu - \xi_L^\mu}\xi^\mu - \frac{\xi_R^\mu + \xi_L^\mu}{\xi_R^\mu - \xi_L^\mu}, \tag{2.15}$$

that maps the physical coordinate ξ^μ onto the collocation coordinate η^μ [62]. Therefore for the derivatives, we will have

$$\begin{cases} \dfrac{\partial^{(p)}u^\mu(\xi^\mu, t)}{\partial\xi^{\mu,(p)}} = \left(\dfrac{2}{\xi_R^\mu - \xi_L^\mu}\right)^p \dfrac{\partial^{(p)}u^\mu(\eta^\mu, t)}{\partial\eta^{\mu,(p)}} \\ \quad \simeq \left(\dfrac{2}{\xi_R^\mu - \xi_L^\mu}\right)^p \{\Phi^\mu{}_{[0:N]}D^{\mu,(p)}_{[0:N,0:N]}\}\hat{\mathbf{u}}^\mu, \\ \dfrac{\partial^{(p)}v^\mu(\xi^\mu, t)}{\partial\xi^{\mu,(p)}} = \left(\dfrac{2}{\xi_R^\mu - \xi_L^\mu}\right)^p \dfrac{\partial^{(p)}v^\mu(\eta^\mu, t)}{\partial\eta^{\mu,(p)}} \\ \quad \simeq \left(\dfrac{2}{\xi_R^\mu - \xi_L^\mu}\right)^p \{\Phi^\mu{}_{[0:N]}D^{\mu,(p)}_{[0:N,0:N]}\}\hat{\mathbf{v}}^\mu, \end{cases} \tag{2.16}$$

where D^μ is the differential matrix on the element Ω^μ and $[D^\mu]_{jk} = \frac{d\phi_k^\mu}{d\eta^\mu}(\eta_j^\mu)$. For computing the entries of differentiation matrix $D^{\mu,(p)}$, $p \geq 1$, we use the recursive formula which is presented in [63,64].

Consider the grid points $\{\xi_0^1, \ldots, \xi_{N-1}^1 = \xi_0^2, \xi_N^1 = \xi_1^2, \ldots, \xi_{N-1}^{\mu-1} = \xi_0^\mu, \xi_N^{\mu-1} = \xi_1^\mu, \ldots, \xi_N^M\}$ where $\xi_j^\mu = \ell/2\eta_j^\mu + \ell/2 + \xi_0^\mu$, $\xi_0^1 = \xi_L$, $\xi_N^M = \xi_R$. The interpolation of function u to arbitrary position ξ in the internal $[\xi_L, \xi_R]$ could be written as

$$u(\xi) = \tilde{\Phi}_{[0:M(N-1)+1]}\mathbf{u}, \tag{2.17}$$

where the vectors $\tilde{\Phi}$ and $\mathbf{u}$ consist of joining the vectors $\hat{\mathbf{u}}^{(\mu)}$ and Φ^μ as follows:

$$\tilde{\Phi}_{[0:M(N-1)+1]} = [\phi_0^1(\eta^1), \ldots, \phi_{N-1}^1(\eta^1), \phi_1^2(\eta^2), \ldots, \phi_{N-1}^\mu(\eta^\mu), \phi_1^{\mu+1}(\eta^{\mu+1}), \ldots, \phi_{N-1}^M(\eta^M), \phi_N^M(\eta^M)],$$
$$\mathbf{u} = [\tilde{u}_0^1(t), \ldots, \tilde{u}_{N-1}^1(t), \tilde{u}_1^2(t), \ldots, \tilde{u}_{N-1}^\mu(t), \tilde{u}_1^{\mu+1}(t), \ldots, \tilde{u}_{N-1}^M(t), \tilde{u}_N^M(t)]^T.$$

With these definitions, we will have

$$\frac{d^{(p)}u(\xi)}{d\xi^{(p)}} = (\tilde{\Phi}_{[0:M(N-1)+1]}\tilde{D}^{(p)}_{[0:M(N-1)+1,0:M(N-1)+1]})\mathbf{u}, \tag{2.18}$$

where

$$\begin{cases} \tilde{D}^{(p)}_{[0:N-1,0:N]} = (2/\ell)^p D^{1,(p)}_{[0:N-1,0:N]}, \\ \tilde{D}^{(p)}_{[\mu(N-1)+1:(\mu+1)(N-1),\mu(N-1):(\mu+1)(N-1)+1]} \\ \quad = (2/\ell)^p D^{\mu+1,(p)}_{[1:N-1,0:N]}, \quad \mu = 1, 2, \ldots, M-2, \\ \tilde{D}^{(p)}_{[(M-1)(N-1)+1:M(N-1)+1,(M-1)(N-1):M(N-1)+1]} \\ \quad = (2/\ell)^p D^{M,(p)}_{[1:N,0:N]}, \end{cases}$$

and the remaining components of the matrix $\tilde{D}^{(p)}_{(M(N-1)+2)\times(M(N-1)+2)}$ are zero. Note that, the above matrix, with large M, is sparse but the matrix becomes full if only a single domain is used in the calculations [33,60,56,57].

To solve the system (2.8)–(2.10), using (2.12)–(2.18) and collocating (2.8) and (2.9) at the $M(N-1)$ interior points $\{\xi_1^1, \ldots, \xi_{N-1}^1, \xi_1^2, \ldots, \xi_{N-1}^{\mu-1}, \xi_1^\mu, \ldots, \xi_{N-1}^M\}$, and also applying (2.10) at two boundary points ξ_0^1 and ξ_N^M lead to a linear system of algebraic equations as follows

$$(\mathbf{A}\otimes\mathbf{B} + \mathbf{C})\mathbf{Y}^{n+1} = (-\mathbf{A}\otimes\mathbf{B} + \mathbf{C})\mathbf{Y}^n + \mathbf{f}, \tag{2.19}$$

where

$$\mathbf{Y}(t) = [\tilde{v}_1^1(t), \ldots, \tilde{v}_{N-1}^1(t), \tilde{v}_1^2(t), \ldots, \tilde{v}_{N-1}^M(t), \tilde{u}_1^1(t), \ldots, \tilde{u}_{N-1}^1(t), \tilde{u}_1^2(t), \ldots, \tilde{u}_{N-1}^M(t)]^T,$$
$$\mathbf{Y}^n = \mathbf{Y}(t_n), \qquad \mathbf{Y}^{n+1} = \mathbf{Y}(t_n + \tau),$$
$$\mathbf{A} = \begin{bmatrix} \delta & 0 \\ 0 & -\delta \end{bmatrix}, \qquad \mathbf{B} = \tilde{D}^{(2)}_{[1:M(N-1),1:M(N-1)]},$$

$$\begin{cases} \mathbf{C}_{[1:M(N-1),1:M(N-1)]} = \mathbf{O}_{[1:M(N-1),1:M(N-1)]}, \\ \mathbf{C}_{[1:M(N-1),M(N-1)+1:2M(N-1)]} = \mathbf{I}_{[1:M(N-1),1:M(N-1)]}, \\ \mathbf{C}_{[M(N-1)+1:2M(N-1),1:M(N-1)]} = \mathbf{I}_{[1:M(N-1),1:M(N-1)]}, \\ \mathbf{C}_{[M(N-1)+1:2M(N-1),M(N-1)+1:2M(N-1)]} = \mathbf{O}_{[1:M(N-1),1:M(N-1)]}. \end{cases}$$

$$\begin{cases} \mathbf{f}_{[1:N-1,1]} = -\delta(2/\ell)^2 D^{1,(2)}_{[1:N-1,0]}(f_{1I}(t_n) + f_{1I}(t_{n+1})), \\ \mathbf{f}_{[N:(M-1)(N-1),1]} = \mathbf{O}_{[1:(M-2)(N-1),1]}, \\ \mathbf{f}_{[(M-1)(N-1)+1:M(N-1),1]} \\ \quad = -\delta(2/\ell)^2 D^{M,(2)}_{[1:N-1,N]}(f_{2I}(t_n) + f_{2I}(t_{n+1})), \\ \mathbf{f}_{[M(N-1)+1:(M+1)(N-1),1]} = \delta(2/\ell)^2 D^{1,(2)}_{[1:N-1,0]}(f_{1R}(t_n) + f_{1R}(t_{n+1})), \\ \mathbf{f}_{[(M+1)(N-1)+1:(2M-1)(N-1),1]} = \mathbf{O}_{[1:(M-2)(N-1),1]}, \\ \mathbf{f}_{[(2M-1)(N-1)+1:2M(N-1),1]} \\ \quad = \delta(2/\ell)^2 D^{M,(2)}_{[1:N-1,N]}(f_{2R}(t_n) + f_{2R}(t_{n+1})), \end{cases}$$

$$f_1(t) = f_{1R}(t) + if_{1I}(t), \qquad f_2(t) = f_{2R}(t) + if_{2I}(t),$$

where the matrices $\mathbf{I}$ and $\mathbf{O}$ are identity matrix and zero matrix, respectively. Fig. 1 shows the location of the nonzero entries in the coefficient matrices in both SDPS ($\mathbf{A}\otimes\mathbf{B}+\mathbf{C}$; $N = 256$, $M = 1$) and MDPS ($\mathbf{A}\otimes\mathbf{B}+\mathbf{C}$; $N = 16$, $M = 16$) methods. Compared with the SDPS method where the coefficient matrix is dense, the coefficient matrix with large elements in the MDPS method can be a sparse matrix (see matrix $\mathbf{B}$ in Eq. (2.19)).

2.3. Numerical scheme for the NLS equation

In this part we obtain the algorithm of the proposed method for the solution of the NLS equation in one and multi-dimensions.

2.3.1. The NLS equation in one dimension

Consider the NLS equation (1.1) in one dimension

$$\psi_t = i\alpha\psi_{x_1x_1} + iw\psi + i\beta|\psi|^2\psi, \quad a \leq x_1 \leq b, t > 0, \tag{2.20}$$

with the initial condition

$$\psi(x_1, 0) = \psi^0(x_1), \tag{2.21}$$

and the boundary conditions

$$\psi(a, t) = g_1(t), \qquad \psi(b, t) = g_2(t). \tag{2.22}$$

In order to solve Eq. (2.20) we split it in the following subproblems

$$\psi_t = \frac{i}{2}(w + \beta|\psi|^2)\psi, \tag{2.23}$$

$$\psi_t = i\alpha\psi_{x_1x_1}, \tag{2.24}$$

$$\psi_t = \frac{i}{2}(w + \beta|\psi|^2)\psi, \tag{2.25}$$

and then we obtain the algorithm of the proposed method.

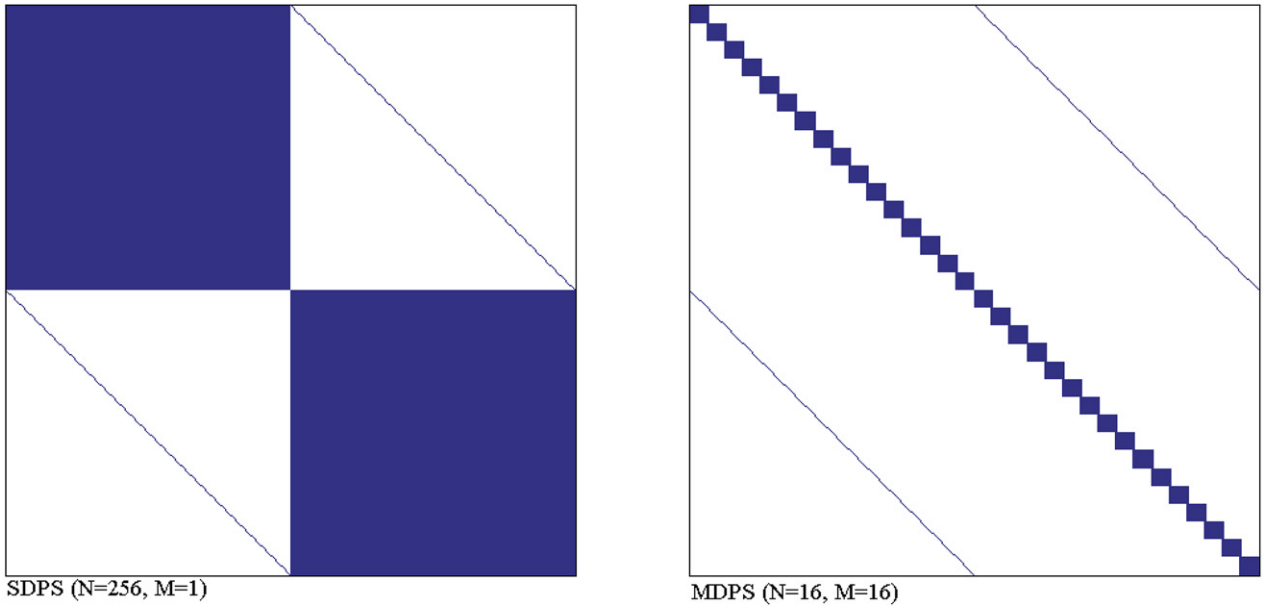

Fig. 1. The graph of the coefficient matrices in both SDPS method ($\mathbf{A}\otimes\mathbf{B}+\mathbf{C}$; $N=256$, $M=1$) and MDPS method ($\mathbf{A}\otimes\mathbf{B}+\mathbf{C}$; $N=16$, $M=16$).

Algorithm 1D. The detailed algorithm of the time-splitting MDPS method for solving Eqs. (2.23)–(2.25), from t_n to t_{n+1} with $n = 0, 1, \ldots$ and $j_{x_1} = 1, 2, \ldots, M_{x_1}(N_{x_1}-1)$, is given in the following

(i) Take $\psi^n_{j_{x_1}}$ as the initial data, solve (2.23) and obtain $\psi^*_{j_{x_1}}$ as follows

$$\psi^*_{j_{x_1}} = \exp[\tau/2(\hat{w}_{j_{x_1}} + \beta|\psi^n_{j_{x_1}}|^2)]\psi^n_{j_{x_1}};$$

(ii) Take $\psi^*_{j_{x_1}}$ as the initial data, solve (2.24) by using (2.19) and obtain $\psi^{**}_{j_{x_1}}$;

(iii) Take $\psi^{**}_{j_{x_1}}$ as the initial data, solve (2.25) and obtain $\psi^{n+1}_{j_{x_1}}$ as follows

$$\psi^{n+1}_{j_{x_1}} = \exp[\tau/2(\hat{w}_{j_{x_1}} + \beta|\psi^{**}_{j_{x_1}}|^2)]\psi^{**}_{j_{x_1}}.$$

2.3.2. NLS equation in multi-dimensions

Since the process of implementation of the proposed method for two and three dimensions is similar then we only demonstrate its algorithm for three dimensions. Consider the NLS equation (1.1) in the three dimensional case.

$$\psi_t = i\alpha(\psi_{x_1x_1} + \psi_{x_2x_2} + \psi_{x_3x_3}) + iw\psi + i\beta|\psi|^2\psi,$$
$$a \le x_1, x_2, x_3 \le b,\ t > 0, \tag{2.26}$$

with the initial condition

$$\psi(x_1, x_2, x_3, t_0) = \psi^0(x_1, x_2, x_3), \tag{2.27}$$

and the boundary conditions

$$\begin{aligned}
&\psi(a, x_2, x_3, t) = g_1(x_2, x_3, t),\\
&\psi(b, x_2, x_3, t) = g_2(x_2, x_3, t),\\
&\psi(x_1, a, x_3, t) = g_3(x_1, x_3, t), \qquad \psi(x_1, b, x_3, t) = g_4(x_1, x_3, t),\\
&\psi(x_1, x_2, a, t) = g_5(x_1, x_2, t), \qquad \psi(x_1, x_2, b, t) = g_6(x_1, x_2, t).
\end{aligned} \tag{2.28}$$

To solve Eq. (2.26), we first split it in the following subproblems

$$\psi_t = i/2(w + \beta|\psi|^2)\psi, \tag{2.29}$$
$$\psi_t = i\alpha\psi_{x_1x_1}, \tag{2.30}$$
$$\psi_t = i\alpha\psi_{x_2x_2}, \tag{2.31}$$
$$\psi_t = i\alpha\psi_{x_3x_3}, \tag{2.32}$$
$$\psi_t = i/2(w + \beta|\psi|^2)\psi. \tag{2.33}$$

Now we obtain the algorithm of the proposed method for this problem.

Algorithm 3D. The detailed algorithm of the time-splitting MDPS method for solving Eqs. (2.29)–(2.33), from t_n to t_{n+1} with $n = 0, 1, \ldots$ and $j_{x_k} = 1, 2, \ldots, M_{x_k}(N_{x_k}-1)$; $k = 1, 2, 3$, is given in the following

(i) Take $\psi^n_{j_{x_1},j_{x_2},j_{x_3}}$ as the initial data, solve (2.29) and obtain $\psi^*_{j_{x_1},j_{x_2},j_{x_3}}$ as follows

$$\psi^*_{j_{x_1},j_{x_2},j_{x_3}} = \exp[\tau/2(\hat{w}_{j_{x_1},j_{x_2},j_{x_3}} + \beta|\psi^n_{j_{x_1},j_{x_2},j_{x_3}}|^2)]\psi^n_{j_{x_1},j_{x_2},j_{x_3}},$$

(ii) Take $\psi^*_{j_{x_1},j_{x_2},j_{x_3}}$ as the initial data, solve (2.30) by using (2.19) and obtain $\psi^{**,1}_{j_{x_1},j_{x_2},j_{x_3}}$;

(iii) Take $\psi^{**,1}_{j_{x_1},j_{x_2},j_{x_3}}$ as the initial data, solve (2.31) by using (2.19) and obtain $\psi^{**,2}_{j_{x_1},j_{x_2},j_{x_3}}$;

(iv) Take $\psi^{**,2}_{j_{x_1},j_{x_2},j_{x_3}}$ as the initial data, solve (2.32) by using (2.19) and obtain $\psi^{**,3}_{j_{x_1},j_{x_2},j_{x_3}}$;

(v) Take $\psi^{**,3}_{j_{x_1},j_{x_2},j_{x_3}}$ as the initial data, solve (2.33) and obtain $\psi^{n+1}_{j_{x_1},j_{x_2},j_{x_3}}$ as follows

$$\psi^{n+1}_{j_{x_1},j_{x_2},j_{x_3}} = \exp[\tau/2(\hat{w}_{j_{x_1},j_{x_2},j_{x_3}} + \beta|\psi^{**,3}_{j_{x_1},j_{x_2},j_{x_3}}|^2)]\psi^{**,3}_{j_{x_1},j_{x_2},j_{x_3}}.$$

3. Numerical experiments

In this section some numerical experiments are made to verify efficiency and high accuracy of the present method for various NLS equations with the Dirichlet boundary conditions. For estimating the error of the numerical solution, we use the norm of maximum error defined by

$$L_\infty(R(\psi)) = \max_j |Real(\psi^{exact}_{j,n}) - Real(\psi^{numerical}_{j,n})|,$$
$$L_\infty(I(\psi)) = \max_j |Imaginary(\psi^{exact}_{j,n}) - Imaginary(\psi^{numerical}_{j,n})|,$$

where $\psi_{j,n}$ is the solution at the point $(\mathbf{x}_j, t_n)$. We will also study the long-time behavior of these equations with the proposed method in large scale domains. The numerical experiments are conducted by taking $N_{x_1} = N_{x_2} = N_{x_3} = Npoints$ and $M_{x_1} = M_{x_2} = M_{x_3} =$

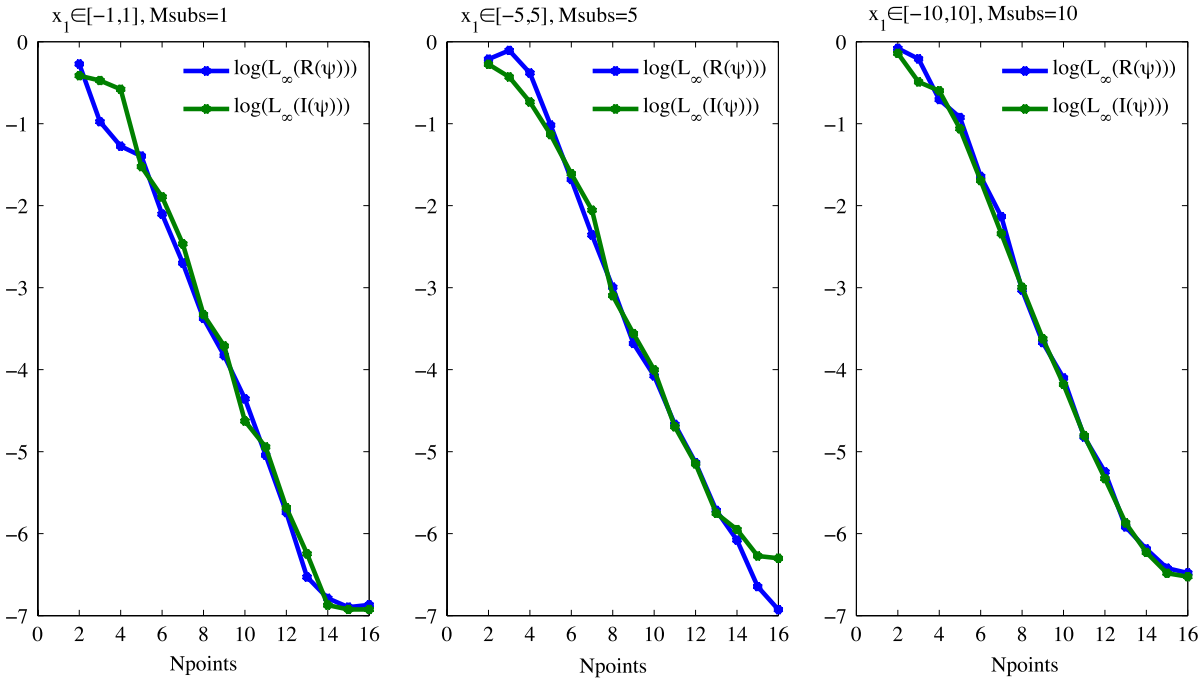

Fig. 2. The relation between the maximum error and Npoints for Problem 1D in Example 1.

Table 1
The maximum error for the numerical solution of Problem 1D in Example 1 at different times.

T	5	10	15	20
$L_\infty(R(\psi))$	4.01E−6	4.83E−6	5.30E−6	6.29E−6
$L_\infty(I(\psi))$	3.82E−6	4.74E−6	5.12E−6	5.37E−6

Table 2
The maximum error for the numerical solution of Problem 2D in Example 1 at different times.

T	1	2	3	4
$L_\infty(R(\psi))$	1.23E−4	1.28E−4	2.75E−4	1.57E−4
$L_\infty(I(\psi))$	1.07E−4	1.32E−4	1.50E−4	2.18E−4

Msubs. The conservation properties for our numerical scheme are examined by calculating discrete analogs of the conserved quantities charge and energy. For studying these conservation laws, we define the functions of charge error and energy error as follows

$$ErrQ(t) = |Q^n - Q^0|,$$
$$ErrE(t) = |E^n - E^0|,$$

where Q^0 and E^0 are the initial charge and energy with $t = 0$ and Q^n and E^n are the discrete quantities charge and energy at $t = n \times \tau$, respectively. Note that, for studying the conservation laws in a limited time interval, we need to choose a sufficiently large domain where the boundary conditions are approximated by zero.

3.1. Example 1

Consider the following Eq. (1.1) with $\beta = 2$ and $w \equiv 0$

$$i\psi_t + \alpha\triangle\psi + 2|\psi|^2\psi = 0, \tag{3.1}$$

with the initial condition

$$\psi^0 = \exp\left(2i\sum_{j=1}^{k} x_j\right)\operatorname{sech}\left(\sum_{j=1}^{k} x_j\right), \quad k = 1, 2. \tag{3.2}$$

We investigate the numerical solution with the proposed method for this example in one and two dimensions where the analytical solution of this equation is in the following form [27]

$$\psi(\mathrm{x}, t) = \exp\left(i\left(2\sum_{j=1}^{k} x_j - 3t\right)\right)\operatorname{sech}\left(\sum_{j=1}^{k} x_j - 4t\right),$$
$$\mathrm{x} = x_1, \ldots, x_k, k = 1, 2, \tag{3.3}$$

and the Dirichlet boundary conditions are directly obtained from the analytical solution.

Problem 1D. We study the following NLS equation (3.1) with $\alpha = 1$ in 1D. To have an overview of the rate of convergence, we plot $\log(L_\infty(R(\psi)))$ and $\log(L_\infty(I(\psi)))$ as a function of *Npoints* at time $t = 1$. In Fig. 2 we observe the errors of the numerical solution in the three intervals $[-1, 1]$, $[-5, 5]$ and $[-10, 10]$ with 1, 5 and 10 elements, respectively. This figure shows that the present method can provide very high accuracy with a large enough number of points. Table 1 gives the maximum error of this numerical solution at different times. In Fig. 3, the numerical simulations of real and imaginary parts, and $|\psi|$ are depicted. It is observed that

Table 3
The maximum error with different mesh sizes in Example 1.

(Npoints, Msubs, τ)	Problem 1D		Problem 2D	
	$L_\infty(R(\psi))$	$L_\infty(I(\psi))$	$L_\infty(R(\psi))$	$L_\infty(I(\psi))$
(16, 4, 0.01)	1.74E−2	1.51E−2	6.15E−2	5.36E−2
(16, 8, 0.001)	1.63E−4	1.09E−4	9.70E−4	8.00E−4
(16, 16, 0.0001)	3.14E−7	2.03E−7	9.02E−5	7.65E−5

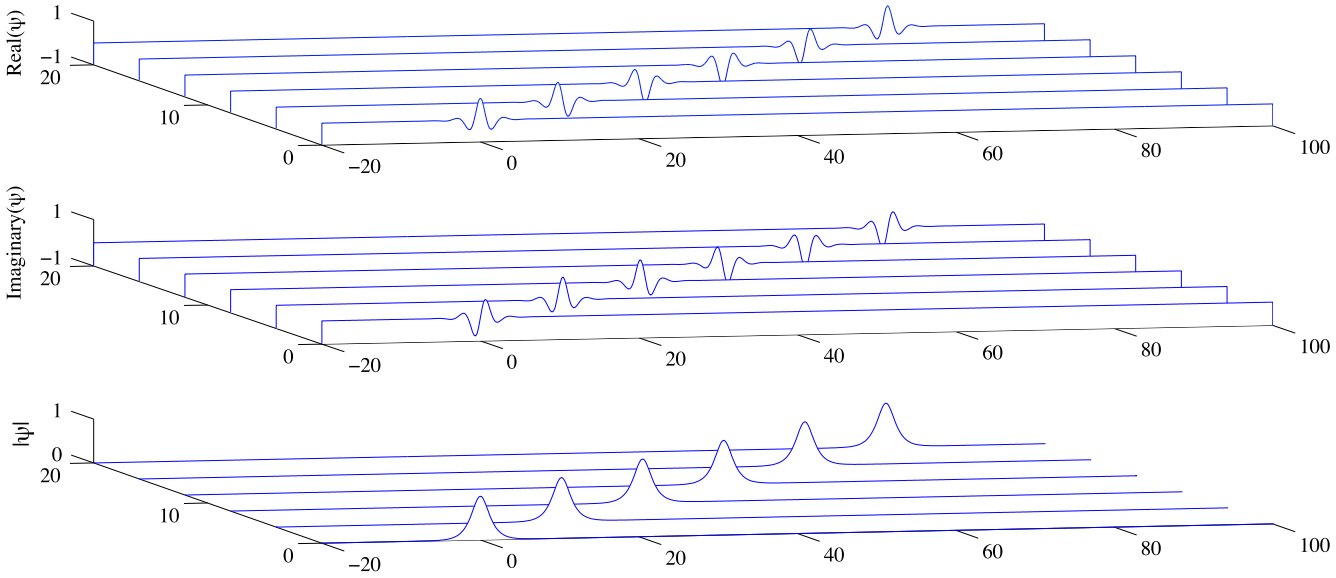

Fig. 3. The space–time graph for the numerical solution of Problem 1D in Example 1 ($(x_1, t) \in [-20, 100] \times [0, 20]$).

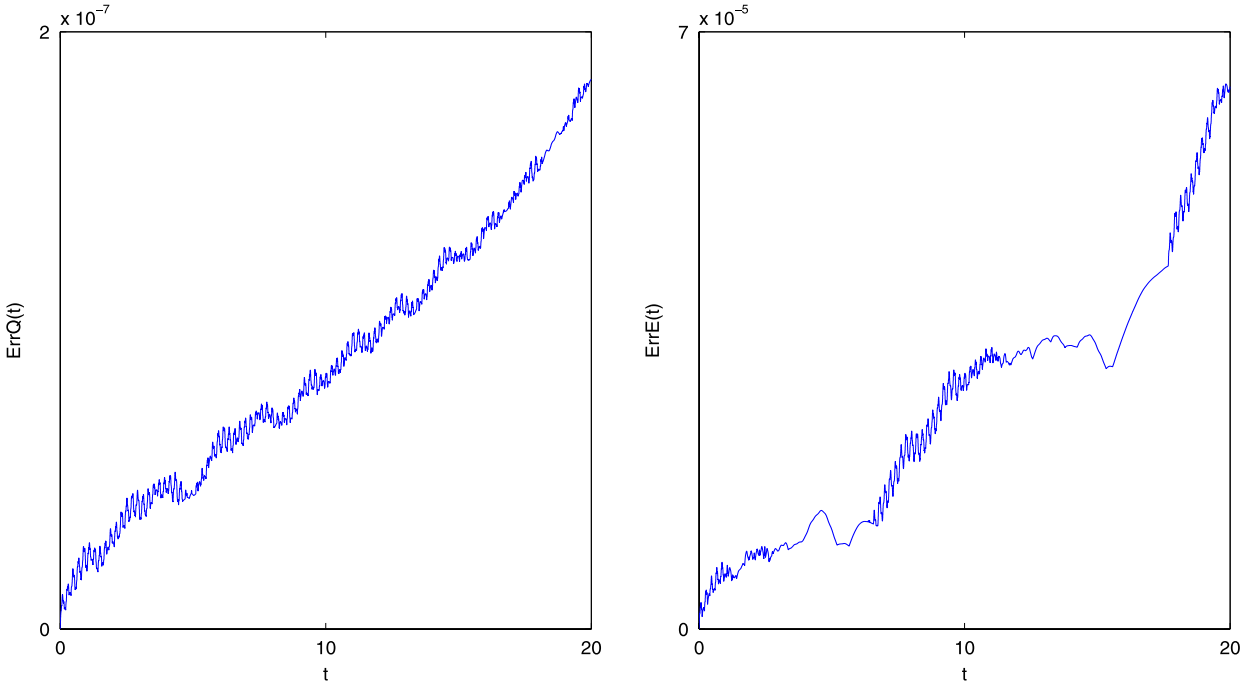

Fig. 4. The variation of the conservation errors of MDPS method for Problem 1D in Example 1.

$|\psi|$ preserves its initial shape during the wave motion from left to right. Also Fig. 4 shows the conservation errors charge and energy in time interval $t \in [0, 20]$. Table 1 and Figs. 3 and 4 report the numerical results in the interval $(x_1, t) \in [-20, 100] \times [0, 20]$ with $Npoints = 30$, $Msubs = 20$ and $\tau = 0.0001$.

Problem 2D. We study the following NLS equation (3.1) with $\alpha = 0.5$ in 2D. The numerical simulations of $|\psi(x_1, x_2, t)|$; $t = 0.5, 1, \ldots, 4$, in the space interval $(x_1, x_2) \in [-10, 10] \times [-10, 10]$ are depicted in Fig. 5 with $Npoints = 16$, $Msubs = 5$ and $\tau = 0.0001$. Also Table 2 reports the maximum error of this numerical solution at times $t = 1, 2, 3$ and 4.

In Table 3, the comparison of numerical results is presented for this example in both one and two dimensions with different mesh sizes. In this table we set the space interval $x_k \in [-16, 16]$, $k = 1, 2$ at time $t = 0.5$.

3.2. Example 2

Consider the following NLS equation (3.1) with the initial condition

$$\psi^0 = 0.5 \exp\left(i \sum_{j=1}^{k} x_j\right) \tanh\left(\left(\sum_{j=1}^{k} x_j\right) \Big/ \sqrt{2}\right), \quad k = 1, 2. \tag{3.4}$$

We investigate the numerical solution with the proposed method for this example in one and two dimensions where the analytical solution of this equation is in the following form [27]

$$\psi(x, t) = 0.5 \exp\left(i\left(\sum_{j=1}^{k} x_j + t\right)\right)$$

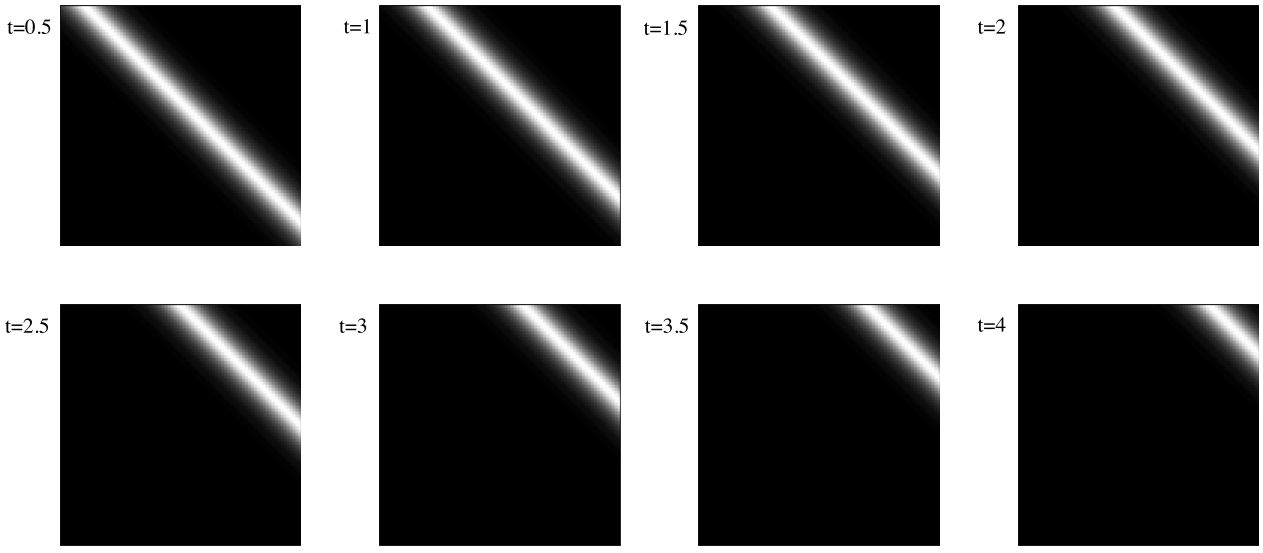

Fig. 5. Images $|\psi(x_1, x_2, t)|$ for the numerical solution of Problem 2D in Example 1 at times $t = 0.5, 1, \ldots, 4$ ($(x_1, x_2) \in [-10, 10] \times [-10, 10]$).

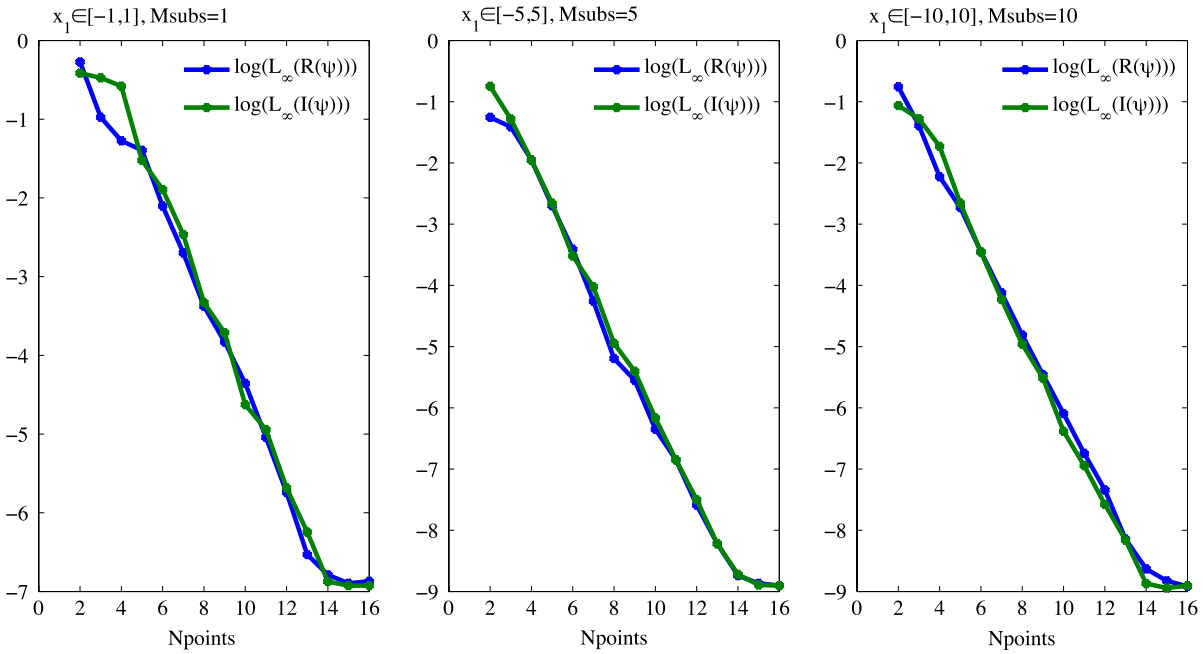

Fig. 6. The relation between the maximum error and *Npoints* for Problem 1D in Example 2.

$$\times \tanh\left(\left(\sum_{j=1}^{k} x_j + t\right)\Big/\sqrt{2}\right),$$

$$x = x_1, \ldots, x_k, k = 1, 2, \tag{3.5}$$

and the Dirichlet boundary conditions are directly obtained from the analytical solution.

Problem 1D. We study the following NLS equation (3.1) with $\alpha = -0.5$ in 1D. Fig. 6 gives the relation between the maximum error and *Npoints* at time $t = 1$. This figure shows the errors of the numerical solution in the three intervals $[-1, 1]$, $[-5, 5]$ and $[-10, 10]$ with 1, 5 and 10 elements, respectively. For this example, we also observe that the present method can be quite accurate with a large enough number of points. The space–time graph of the numerical solution is presented in Fig. 7. This figure shows that the solitary wave transfers from the right to the left as time increases while the initial shape of $|\psi|$ does not change.

Table 4
The maximum error for the solution of Problem 1D in Example 2 at different times.

T	20	40	60	80
$L_\infty(R(\psi))$	9.56E−9	2.73E−8	2.75E−8	3.28E−8
$L_\infty(I(\psi))$	9.22E−9	2.85E−8	1.93E−8	3.97E−8

Also Table 4 gives the maximum error of this numerical solution at different times. Fig. 7 and Table 4 report the numerical results and also Fig. 8 shows the curve errors of the discrete conservation properties, charge and energy, in the interval $(x_1, t) \in [-90, 10] \times [0, 80]$ with $Npoints = 25$, $Msubs = 20$ and $\tau = 0.0001$.

Problem 2D. We study the following NLS equation (3.1) with $\alpha = -0.25$ in 2D. The numerical simulations of $|\psi(x_1, x_2, t)|$ in the space interval $(x_1, x_2) \in [-30, 30] \times [-30, 30]$ and $t = 5, 10, \ldots, 40$ are given in Fig. 9. Table 5 reports the maximum error of this numerical solution at times $t = 10, 20, 30$ and 40. These results also

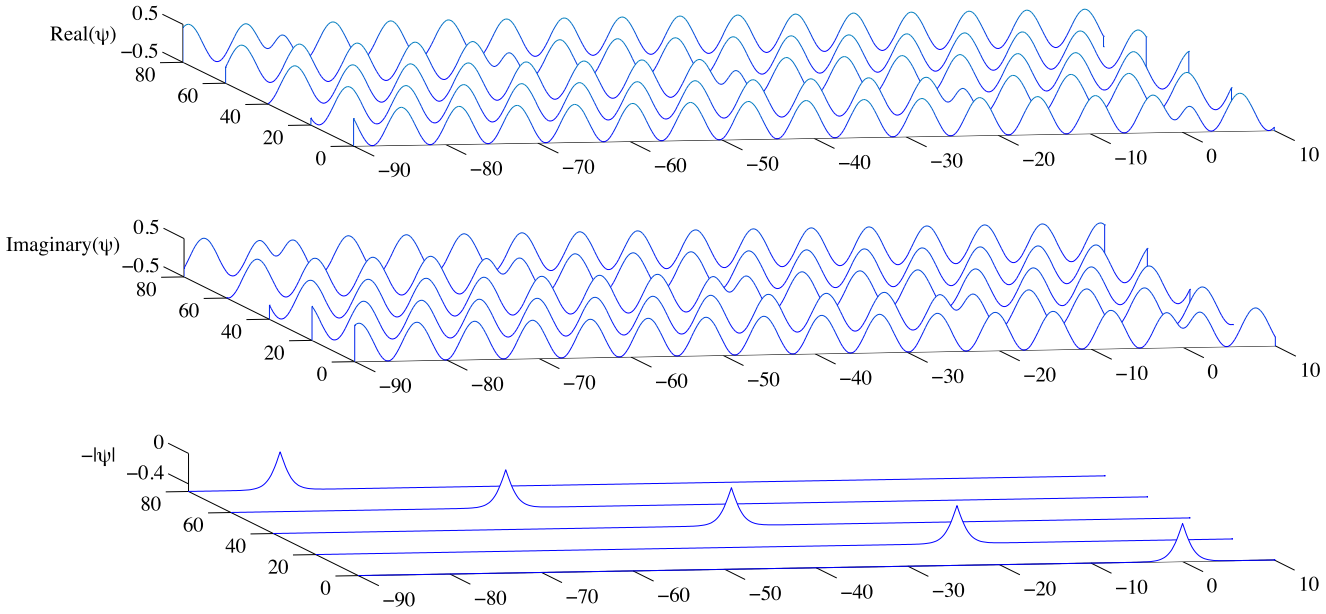

Fig. 7. The space–time graph for Problem 1D in Example 2 ($(x_1, t) \in [-90, 10] \times [0, 80]$).

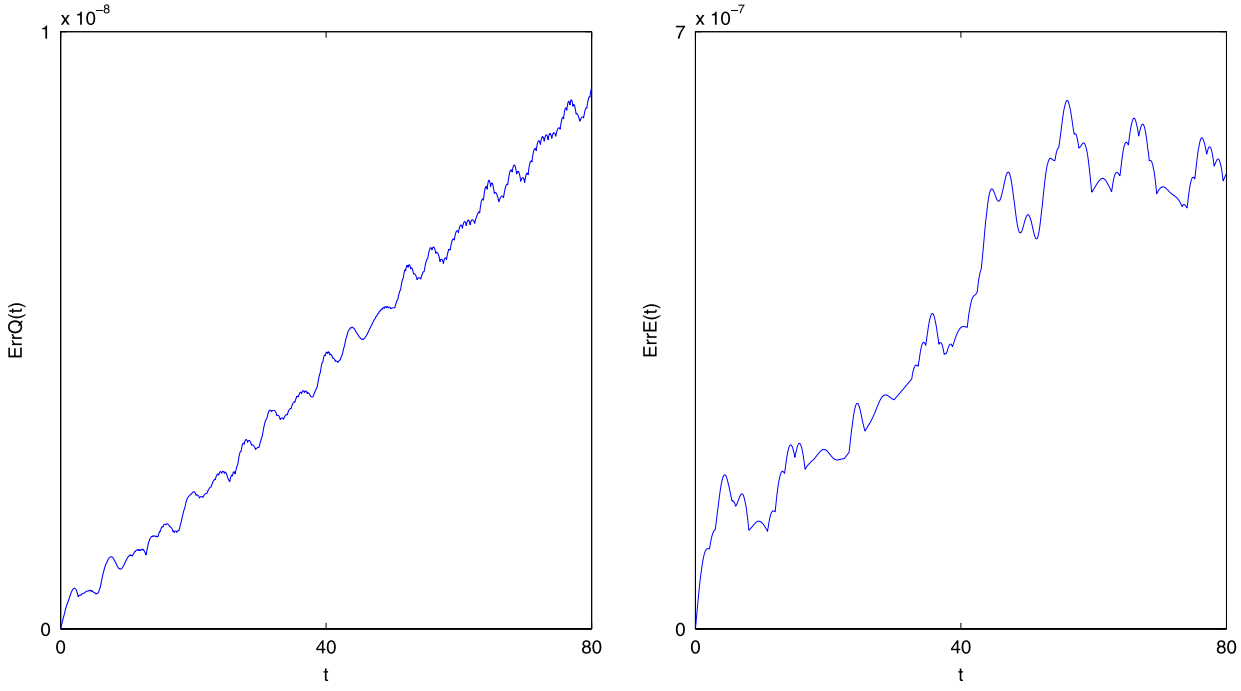

Fig. 8. The variation of the conservation errors of MDPS method for Problem 1D in Example 2.

Table 5
The maximum error for the solution of Problem 2D in Example 2 at different times.

T	10	20	30	40
$L_\infty(R(\psi))$	1.93E−5	1.87E−5	2.20E−5	3.15E−5
$L_\infty(I(\psi))$	1.72E−5	1.75E−5	1.93E−5	2.85E−5

show the efficiency of the present method for long time simulation in two dimensions. In Fig. 9 and Table 5, we set $Npoints = 50$, $Msubs = 4$ and $\tau = 0.0001$.

In Table 6, the comparison of numerical results is reported for this example in both one and two dimensions with different mesh sizes. In this table, we set the space interval $x_k \in [-30, 30]$, $k = 1, 2$ at time $t = 0.5$.

3.3. Example 3

Consider the following Eq. (1.1) with $\alpha = 0.5$ and $\beta = -1$

$$i\psi_t + 0.5\triangle\psi + w\psi - |\psi|^2\psi = 0, \tag{3.6}$$

where the initial condition is

$$\psi^0 = \exp\left(-\sum_{j=1}^{k}((x_j - 8)^2 + ix_j)\right), \quad k = 1, 2, 3. \tag{3.7}$$

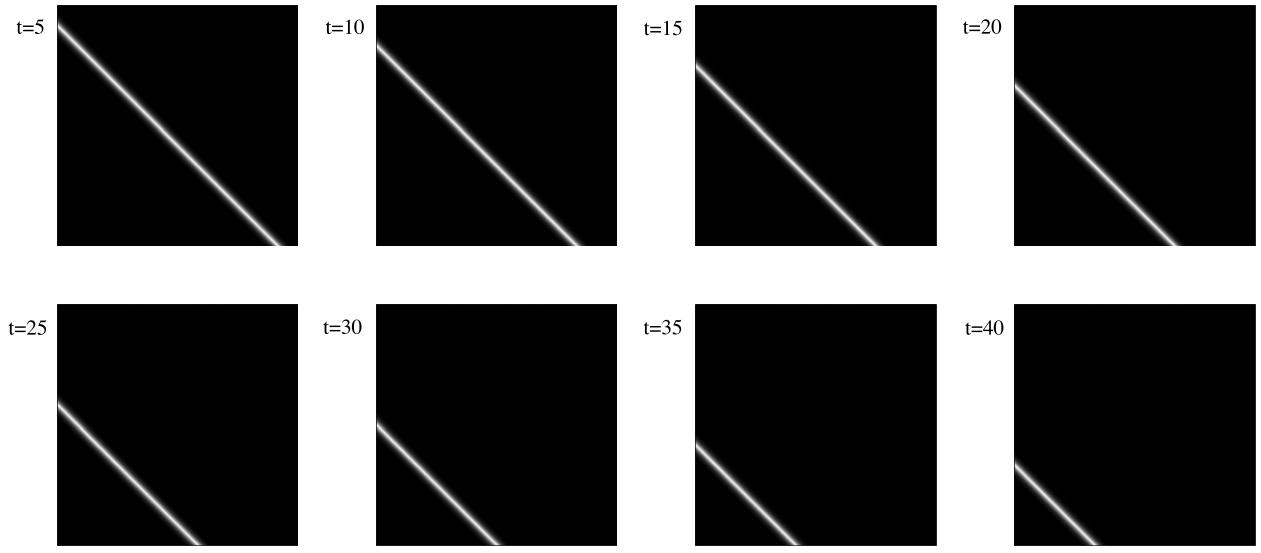

Fig. 9. Images $|\psi(x_1, x_2, t)|$ for the numerical solution of Problem 2D in Example 2 at times $t = 5, 10, \ldots, 40$ ($(x_1, x_2) \in [-30, 30] \times [-30, 30]$).

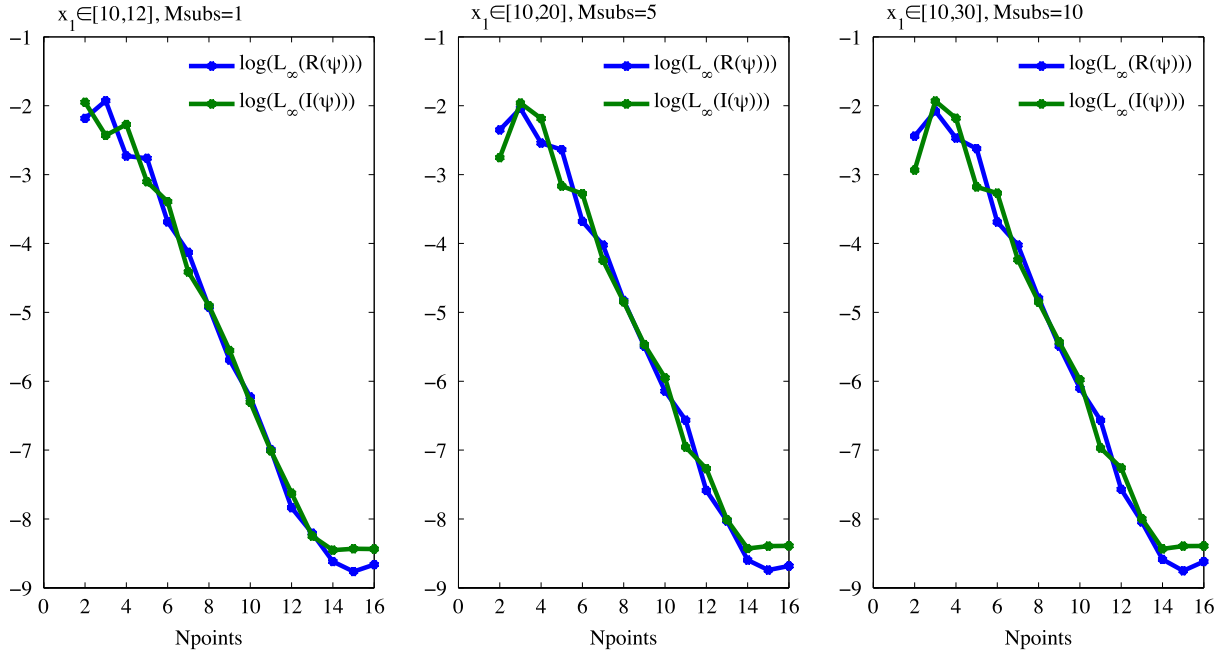

Fig. 10. The relation between the maximum error and *Npoints* for Problem 1D in Example 3.

Table 6
The maximum error with different mesh sizes in Example 2.

(Npoints, Msubs, τ)	Problem 1D		Problem 2D	
	$L_\infty(R(\psi))$	$L_\infty(I(\psi))$	$L_\infty(R(\psi))$	$L_\infty(I(\psi))$
(16, 4, 0.01)	7.85E−4	9.29e−4	1.03E−2	1.81e−2
(16, 8, 0.001)	9.94E−6	3.06e−5	4.90E−4	2.18e−4
(16, 16, 0.0001)	5.91E−8	5.32e−8	2.08E−5	2.11e−5

We test the efficiency and accuracy of the proposed scheme by comparing the analytical solutions in one, two and three dimensions where the analytical solution of this equation is [36]

$$\psi(\mathrm{x}, t) = \exp\left(-\sum_{j=1}^{k}(x_j - 8 - t)^2 + i\left(\sum_{j=1}^{k} x_j - t\right)\right),$$
$$\mathrm{x} = x_1, \ldots, x_k, \; k = 1, 2, 3, \tag{3.8}$$

and the Dirichlet boundary conditions are directly obtained from the analytical solution.

Problem 1D. We study the following NLS equation (3.6) in 1D with the potential function

$$w(x_1, t) = 0.5 - 2(x_1 - 8 - t)^2 + \exp(-2(x_1 - 8 - t)^2). \tag{3.9}$$

Like the previous examples, in this case we also study the relation between the maximum error and *Npoints* at time $t = 1$ in Fig. 10.

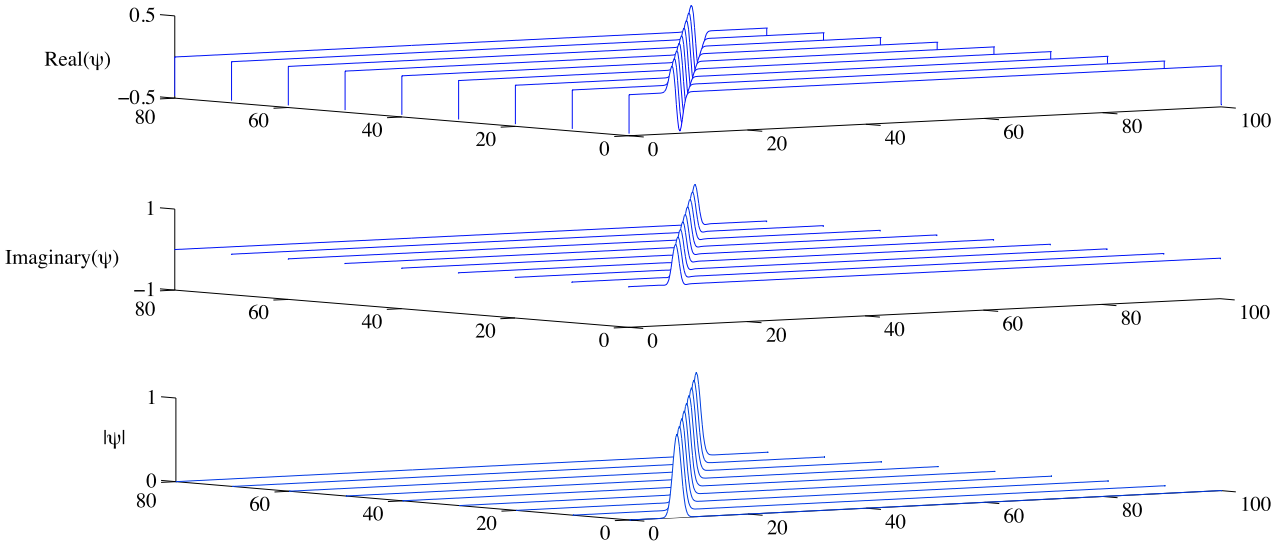

Fig. 11. The space–time graph for Problem 1D in Example 3 ($(x_1, t) \in [0, 100] \times [0, 80]$).

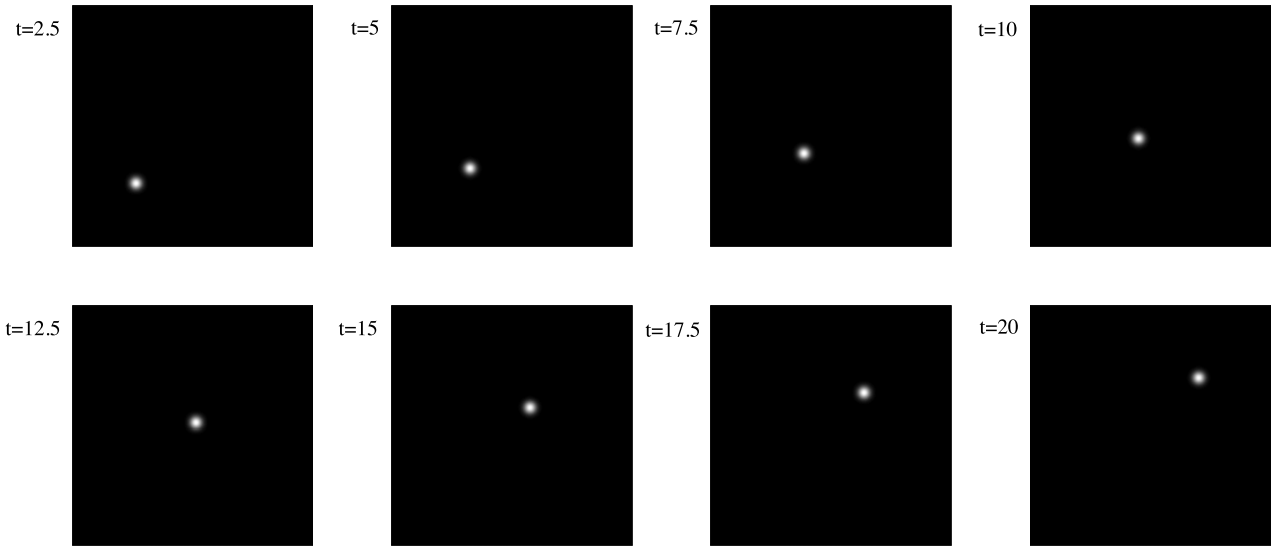

Fig. 12. Images $|\psi(x_1, x_2, t)|$ for the numerical solution of Problem 2D in Example 3 at times $t = 2.5, 5, \ldots, 20$ ($(x_1, x_2) \in [0, 40] \times [0, 40]$).

Table 7
The maximum error for the solution of Problem 1D in Example 3 at different times.

T	20	40	60	80
$L_\infty(R(\psi))$	4.25E−7	1.23E−6	9.48E−7	7.12E−7
$L_\infty(I(\psi))$	4.34E−7	9.16E−7	7.33E−7	2.84E−7

In this figure we observe the errors of the numerical solution in the three intervals [10, 12], [10, 20] and [10, 30], with 1, 5 and 10 elements, respectively. This figure shows that the present method can provide the spectral accuracy with a large enough number of points. It can be observed that the errors of the numerical results are consistent to the above examples. Fig. 11 shows the propagation of the solitary wave in this problem. This figure clearly shows $|\psi|$ preserves the initial shape as time increases. Also Table 7 gives the maximum error of this numerical solution at different times up to $t = 80$. Fig. 11 and Table 7 report the numerical results in the interval $(x_1, t) \in [0, 100] \times [0, 80]$ with $Npoints = 25$, $Msubs = 20$ and $\tau = 0.0001$.

Problem 2D. We study the following NLS equation (3.6) in 2D with the potential function

$$w(x_1, x_2, t) = 2 - 2\sum_{j=1}^{2}(x_j - 8 - t)^2 + \exp\left(-2\sum_{j=1}^{2}(x_j - 8 - t)^2\right). \tag{3.10}$$

The images of numerical simulations $|\psi(x_1, x_2, t)|; t = 2.5, 5, \ldots, 20$, in $(x_1, x_2) \in [0, 40] \times [0, 40]$ are depicted in Fig. 12 with $Npoints = 100$, $Msubs = 2$ and $\tau = 0.0001$. Also Table 8 reports the maximum error of this numerical solution at times $t = 5, 10, 15$ and 20.

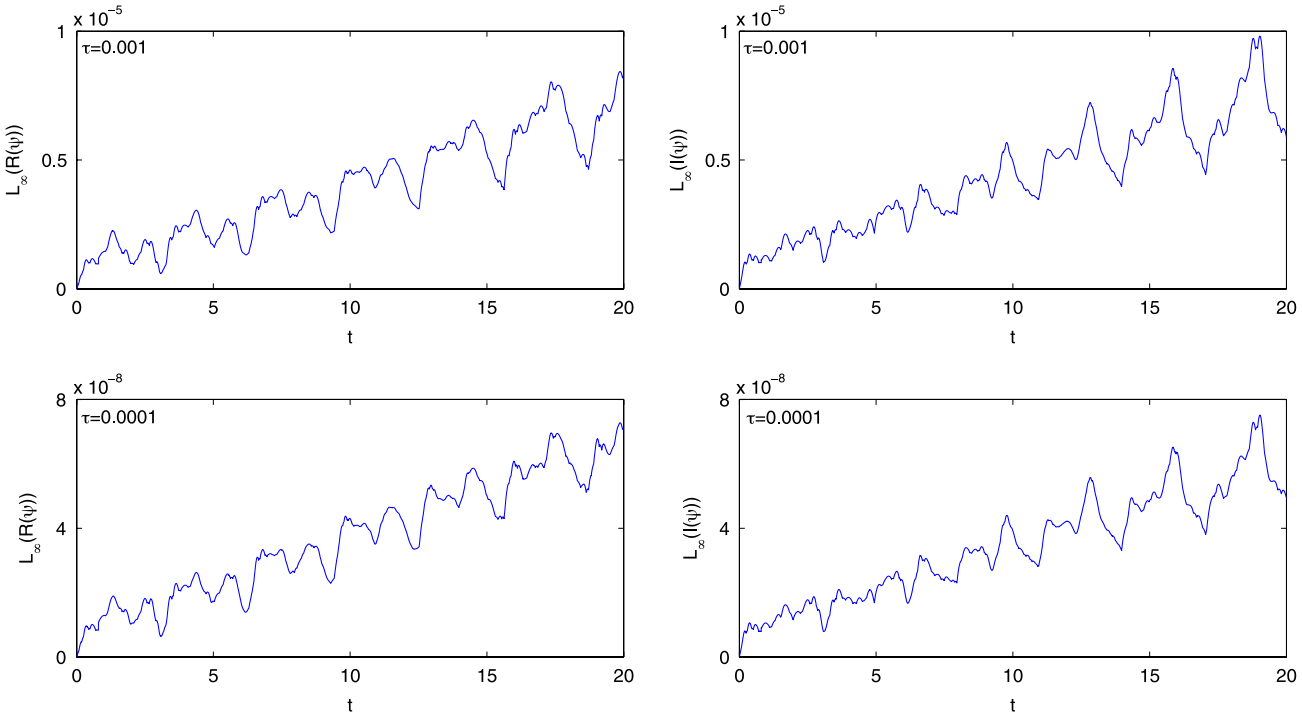

Fig. 13. The maximum error for Problem 3D in Example 3 ($(x_1, x_2, x_3, t) \in [0, 40] \times [0, 40] \times [0, 40] \times [0, 20]$).

Table 8
The maximum error for the numerical solution of Problem 2D in Example 3 at different times.

T	5	10	15	20
$L_\infty(R(\psi))$	1.03E−8	2.57E−8	2.84E−8	4.72E−8
$L_\infty(I(\psi))$	1.15E−8	2.32E−8	3.02E−8	4.21E−8

Problem 3D. We study the following NLS equation (3.6) in 3D with the potential function

$$w(x_1, x_2, x_3, t) = 3.5 - 2\sum_{j=1}^{3}(x_j - 8 - t)^2 + \exp\left(-2\sum_{j=1}^{3}(x_j - 8 - t)^2\right). \quad (3.11)$$

Fig. 13 depicts the behavior of maximum error for the numerical solution of Problem 3D at different step sizes in time up to $t = 20$ in $(x_1, x_2, x_3) \in [0, 40] \times [0, 40] \times [0, 40]$ with $Npoints = 50$ and $Msubs = 4$. As shown in this figure, the proposed method gives high accurate results even if we consider long time interval. It also shows that small step size τ can obtain higher accuracy.

In Table 9 we present the maximum error of the numerical solution in the interval $x_k \in [0, 20]$, $k = 1, 2, 3$ at time $t = 1$ for the three problems in Example 3. In this table, various step sizes with fixed time are tested. We also investigate the behavior of the maximum error in this example for the large interval $x_k \in [0, 120]$, $k = 1, 2, 3$ with different mesh sizes at time $t = 0.5$, see Table 10. Fig. 14 includes tests for the discrete charge conservation law in one, two and three dimensions from $t = 0$ to $t = 20$ where we set $x_k \in [0, 40]$, $k = 1, 2, 3$ and $(Npoints, Msubs, \tau) = (50, 4, 0.0001)$. As can be seen from the figures and tables, the obtained results of the proposed method are in a good agreement with the exact solution, even at large values of time and space.

4. Conclusion

In this paper, we studied an efficient and stable method for the numerical solution of the nonlinear Schrödinger equation in one, two and three dimensions. To avoid solving the nonlinear partial differential equation, we applied the Strang splitting method. To

Table 9
The maximum error with different step sizes in Example 3.

	$\tau = 0.01$		$\tau = 0.001$		$\tau = 0.0001$	
	$L_\infty(R(\psi))$	$L_\infty(I(\psi))$	$L_\infty(R(\psi))$	$L_\infty(I(\psi))$	$L_\infty(R(\psi))$	$L_\infty(I(\psi))$
1D	5.6E−5	4.3E−5	7.1E−7	6.3E−7	8.2E−9	2.8E−9
2D	7.3E−5	6.2E−5	7.5E−7	5.4E−7	8.7E−9	5.1E−9
3D	1.0E−4	8.2E−5	1.3E−6	7.1E−7	2.9E−8	7.8E−9

Table 10
The maximum error with different mesh sizes in Example 3.

	$(Npoints = 300, Msubs = 2, \tau = 0.001)$		$(Npoints = 150, Msubs = 2, \tau = 0.01)$	
	$L_\infty(R(\psi))$	$L_\infty(I(\psi))$	$L_\infty(R(\psi))$	$L_\infty(I(\psi))$
1D	6.2E−7	5.9e−7	6.4E−5	5.6e−5
2D	8.3E−7	7.9e−7	7.0E−5	7.8e−5
3D	9.1E−7	8.7e−7	9.8E−5	8.1e−5

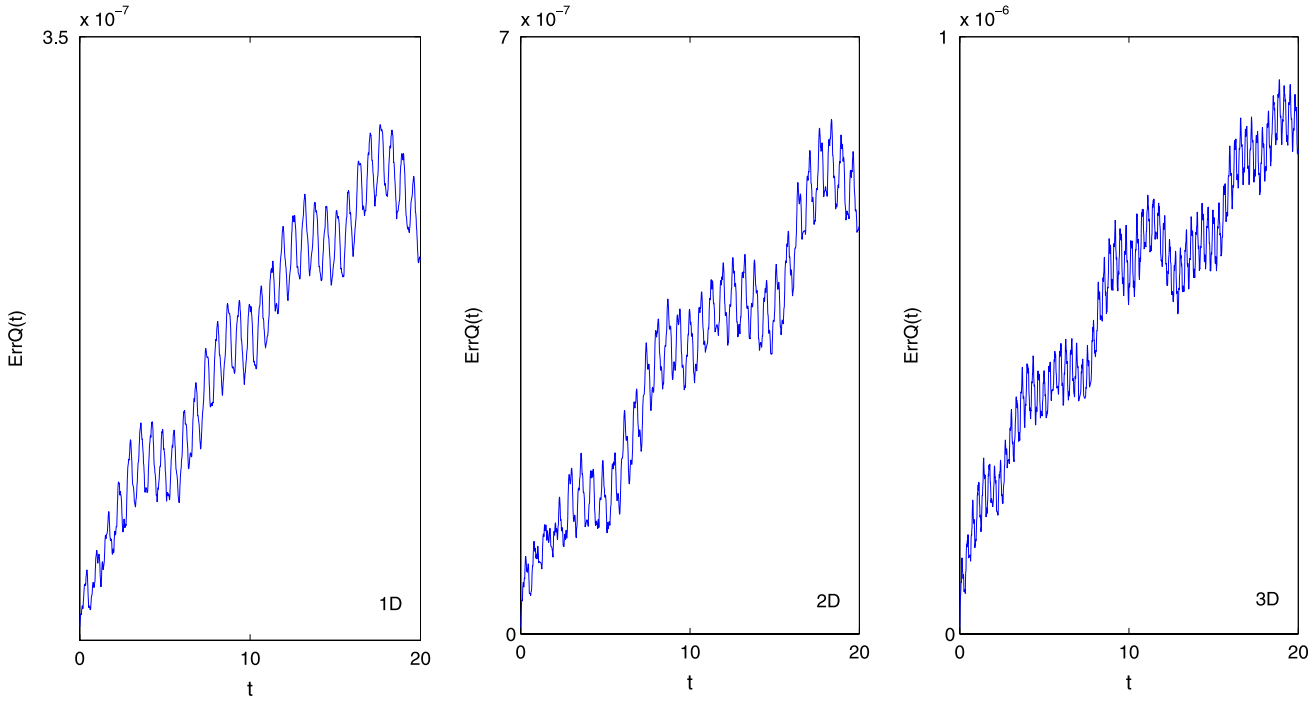

Fig. 14. The variation of the charge conservation error of MDPS method for Problems 1D, 2D and 3D in Example 3.

deal with the high dimensional cases, we employed the alternating direction implicit (ADI) technique. This technique makes contributions in many multi-dimensional problems because of its efficiency in saving CPU time and computer memory. In this paper, at each time step, the nonlinear Schrödinger equation was decoupled into a nonlinear ordinary differential equation and a linear partial differential equation. The nonlinear ordinary differential equation was explicitly calculated. Applying ADI technique, the linear partial differential equation in high dimensions was reduced to equations in one dimension. For the linear partial differential equation in one dimension, we employed an overlapping multi-domain pseudo-spectral method for the approximation in the space variable and the Crank–Nicolson method in time derivative. Using the multi-domain scheme in space variable, the matrices arising in the corresponding problem can be sparse, reducing the computation storage more than the single-domain, especially in high dimensional problems. According to numerical experiments, we find that the present method provides quite accurate results in one and high dimensions and even in some cases we find spectral accuracy for large computational domains. Numerical results also show that the proposed method preserves conserved quantities charge and energy.

Acknowledgments

We would like to express our thanks to both reviewers for their valuable comments and suggestions which helped to improve this paper.

References

[1] Y.V. Kartashov, B.A. Malomed, L. Torner, Solitons in nonlinear lattices, Rev. Modern Phys. 83 (2011) 247–305.
[2] Y.S. Kivshar, G.P. Agrawal, Optical Solitons: From Fibers to Photonic Crystals, Elsevier Science, 2003.
[3] A. Hasegawa, F. Tappert, Transmission of stationary nonlinear optical pulses in dispersive dielectric fibers. I. Anomalous dispersion, Appl. Phys. Lett. 23 (1973) 142–144.
[4] L.F. Mollenauer, R.H. Stolen, J.P. Gordon, Experimental observation of picosecond pulse narrowing and solitons in optical fibers, Phys. Rev. Lett. 45 (1980) 1095–1098.
[5] S. Maneuf, R. Desailly, C. Froehly, Stable self-trapping of laser beams: observation in a nonlinear planar waveguides, Opt. Commun. 65 (1988) 193–198.
[6] G.C. Duree, J.L. Shultz, G.J. Salamo, M. Segev, A. Yariv, B. Crosignani, P. Di Porto, E.J. Sharp, R.R. Neurgaonkar, Observation of self-trapping of an optical beam due to the photorefractive effect, Phys. Rev. Lett. 71 (1993) 533–536.
[7] W.E. Torruellas, Z. Wang, D.J. Hagan, E.W. VanStryland, G.I. Stegeman, L. Torner, C.R. Menyuk, Observation of two-dimensional spatial solitary waves in a quadratic medium, Phys. Rev. Lett. 74 (1995) 5036–5039.
[8] A. Miller, K.R. Welford, B. Daino, Nonlinear optical materials and devices for applications in information technology, in: Proccedings of the NATO Advanced Study Institute, 1995.
[9] M. Dehghan, Finite difference procedures for solving a problem arising in modeling and design of certain optoelectronic devices, Math. Comput. Simulation 71 (2006) 16–30.
[10] G.L. Lamb, Elements of Soliton Theory, Wiely, New York, 1980.
[11] A.M. Wazwaz, Partial Differential Equations and Solitary Waves Theory, Higher Education Press, Beijin, Springer-Verlag, Berlin, Heidelberg, 2009.
[12] G.P. Agrawal, Nonlinear Fiber Optics, third ed., Academic Press, San Diego, 2001.
[13] E. Lo, C.C. Mei, A numericalstudy of water-wave modulation based on a higher-order nonlinear Schrödinger equation, J. Fluid Mech. 150 (1985) 395–416.
[14] B. Tian, W.R. Shan, C.Y. Zhang, G.M. Wei, Y.T. Gao, Transformations for a generalized variable-coefficient nonlinear Schrödinger model from plasma physics, arterial mechanics and optical fibers with symbolic computation, Eur. Phys. J. B 47 (2005) 329–332.
[15] N. Lazarides, G.P. Tsironis, Coupled nonlinear Schrödinger field equations for electromagnetic wave propagation in nonlinear left-handed materials, Phys. Rev. E 71 (2005) 036614.
[16] C. Nore, A. Abid, M. Brachet, Small-Scale Structures in Three-Dimensional Hydrodynamics and Magnetohyrodynamic Turbulence, Springer, Berlin, 1996.
[17] M.A. Helal, Soliton solution of some nonlinear partial differential equations and its application in fluid mechanics, Chaos Solitons Fractals 13 (2002) 1917–1929.
[18] W.K. Abousalem, Solitary wave dynamics in time-dependent potentials, J. Math. Phys. 49 (2008) 032101.
[19] M. A de Moura, Nonlinear Schrödinger solitons in the presence of an external potential, J. Phys. A: Math. Gen. 27 (1994) 7157–7164.
[20] J. Fröhlich, S. Gustafson, B.L.G. Jonsson, I.M. Sigal, Solitary wave dynamics in an external potential, Comm. Math. Phys. 250 (2004) 613–642.
[21] Y. Wang, R. Hao, Exact spatial soliton solution for nonlinear Schrödinger equation with a type of transverse nonperiodic modulation, Opt. Commun. 282 (2009) 3995–3998.
[22] A.G. Bratsos, A modified numerical scheme for the cubic Schrödinger equation, Numer. Methods Partial Differential Equations 27 (2011) 608–620.
[23] I. Dag, A quadratic B-spline finite element method for solving nonlinear Schrödinger equation, Comput. Methods Appl. Mech. Engrg. 174 (1999) 247–258.
[24] Z. Gao, S. Xie, Fourth-order alternating direction implicit compact finite difference schemes for two-dimensional Schrödinger equations, Appl. Numer. Math. 61 (2011) 593–614.

[25] H.L. Liao, Z.Z. Sun, H.S. Shi, Error estimate of fourth-order compact scheme for linear schrödinger equations, SIAM J. Numer. Anal. 47 (2010) 4381–4401.
[26] H.Q. Wang, Numerical studies on the split-step finite difference method for nonlinear Schrödinger equations, Appl. Math. Comput. 170 (2005) 17–35.
[27] H.Q. Wang, An efficient Chebyshev–Tau spectral method for Ginzburg–Landau–Schrödinger equations, Comput. Phys. Commun. 181 (2010) 325–340.
[28] H. Zhu, Y. Chen, S. Song, H. Hu, Symplectic and multisymplectic wavelet collocation methods for two-dimensional Schrödinger equations, Appl. Numer. Math. 61 (2011) 308–321.
[29] L. Kong, Y. Duan, L. Wang, X. Yin, Y. Ma, Spectral-like resolution compact ADI finite difference method for the multi-dimensional Schrödinger equation, Math. Comput. Model. 55 (2012) 1798–1812.
[30] X. Antoine, C. Besse, P. Klein, Numerical solution of time-dependent nonlinear Schrödinger equations using domain truncation techniques coupled with relaxation scheme, Las. Phys. 21 (2011) 1–12.
[31] A.P. Fordy, Soliton Theory: A Survey of Results, Manchester University Press, Manchester, 1990.
[32] J.B. Chen, M.Z. Qin, Y.F. Tang, Symplectic and multi-symplectic methods for the nonlinear Schrödinger equation, Comput. Math. Appl. 43 (2002) 1095–1106.
[33] M. Dehghan, A. Taleei, A Chebyshev pseudo-spectral multi-domain method for the soliton solution of coupled nonlinear Schrödinger equations, Comput. Phys. Commun. 182 (2011) 2519–2529.
[34] M. Dehghan, D. Mirzaei, The meshless local Petrov–Galerkin method (MLPG) for nonlinear two dimensional Schrödinger equation, Engng. Anal. Bound. Elms. 32 (2008) 747–756.
[35] Y. Xu, L. Zhang, Alternating direction implicit method for solving two-dimensional cubic nonlinear Schrödinger equation, Comput. Phys. Commun. 183 (2012) 1082–1093.
[36] S. Wang, L. Zhang, Split-step orthogonal spline collocation methods for nonlinear Schrödinger equations in one, two, and three dimensions, Appl. Math. Comput. 218 (2011) 1903–1916.
[37] M. Dehghan, F. Emami-Naeini, The Sinc-collocation and Sinc–Galerkin methods for solving the two-dimensional Schrödinger equation with nonhomogeneous boundary conditions, Appl. Math. Model. 37 (2013) 9379–9397.
[38] M. Dehghan, D. Mirzaei, Numerical solution to the unsteady two-dimensional Schrödinger equation using meshless local boundary integral equation method, Int. J. Numer. Methods Eng. 76 (2008) 501–520.
[39] M. Dehghan, A. Shokri, A numerical method for two-dimensional Schrödinger equation using collocation and radial basis functions, Comput. Math. Appl. 54 (2007) 136–146.
[40] A. Mohebbi, M. Dehghan, The use of compact boundary value method for the solution of two-dimensional Schrödinger equation, J. Comput. Appl. Math. 225 (2009) 124–134.
[41] J.P. Boyd, Chebyshev and Fourier Spectral Methods, Springer-Verlag, Berlin, New York, 1989.
[42] J.A.C. Weideman, B.M. Herbst, Split-step methods for the solution of the nonlinear Schrödinger equation, SIAM J. Numer. Anal. 23 (1986) 485–507.
[43] P. Muruganandam, S.K. Adhikari, Bose–Einstein condensation dynamics in three dimensions by the pseudo-spectral and finite difference methods, J. Phys. B 36 (2003) 2501–2513.
[44] W. Bao, D. Jaksch, P.A. Markowich, Numerical solution of the Gross–Pitaevskii equation for Bose–Einstein condensation, J. Comput. Phys. 187 (2003) 318–342.
[45] J. Shen, L.L. Wang, Fourierization of the Legendre–Galerkin method and a new space–time spectral method, Appl. Numer. Math. 57 (2007) 710–720.
[46] G. Strang, On the construction and comparison of difference scheme, SIAM J. Numer. Anal. 5 (1968) 506–517.
[47] D. Bai, L. Zhang, Numerical studies on a novel split-step quadratic B-spline finite element method for the coupled Schrödinger-KdV equations, Commun. Nonlinear Sci. Numer. Simul. 16 (2011) 1263–1273.
[48] W. Bao, J. Shen, A fourth-order time splitting Lagurre–Hermite pseudo-spectral method for Bose–Einstein condensates, SIAM J. Sci. Comput. 26 (2005) 2010–2028.
[49] P. Degond, S. Jin, M. Tang, On the time splitting spectral method for the complex Ginzburg–Landau equation in the large time and space scale limit, SIAM J. Sci. Comput. 30 (2008) 2466–2487.
[50] A. Kassam, L.N. Trefethen, Fourth-order time-stepping for stiff PDEs, SIAM J. Sci. Comput. 26 (2005) 1214–1233.
[51] T.F. Chan, L. Shen, Stability analysis of difference schemes for variable coefficient Schrödinger type equations, SIAM J. Numer. Anal. 24 (1987) 336–349.
[52] F. Fakhar-Izadi, M. Dehghan, The spectral methods for parabolic Volterra integro–differential equations, J. Comput. Appl. Math. 235 (2011) 4032–4046.
[53] F. Fakhar-Izadi, M. Dehghan, An efficient pseudospectral Legendre–Galerkin method for solving a nonlinear partial integro–differential equation arising in population dynamics, Math. Methods Appl. Sci. 36 (2013) 1485–1511.
[54] M. Dehghan, F. Fakhar-Izadi, The spectral collocation method with three different bases for solving a nonlinear partial differential equation arising in modeling of nonlinear waves, Math. Comput. Modelling 53 (2011) 1865–1877.
[55] R. Peyret, The Chebyshev multidomain approach to stiff problems in fluid mechanics, Comput. Methods Appl. Mech. Engrg. 80 (1990) 129–145.
[56] H.H. Yang, B.D. Shizgal, Chebyshev pseudospectral multidomain technique for viscous flow calculation, Comput. Methods Appl. Mech. Engrg. 118 (1994) 47–61.
[57] H.H. Yang, B.R. Seymour, B.D. Shizgal, A Chebyshev pseudospectral multidomain method for steady flow past a cylinder, up to $Re = 150$, Comput. Fluids 23 (1994) 829–851.
[58] I.M. Kuria, P.E. Raad, An implicit multidomain spectral collocation method for stiff highly nonlinear fluid dynamics problems, Comput. Meth. Appl. Mech. Engrg. 120 (1995) 163–182.
[59] H.P. Pfeiffer, L.E. Kidder, M.A. Scheel, S.A. Teukolsky, A multi-domain spectral method for solving elliptic equations, Comput. Phys. Commun. 152 (2003) 253–273.
[60] D. Olmos, B.D. Shizgal, A pseudo-spectral method of solution of Fisher's equation, J. Comput. Appl. Math. 193 (2006) 219–242.
[61] S. Blanes, P.C. Moan, Splitting methods for the time-dependent Schrödinger equation, Phys. Lett. A 265 (2000) 32–42.
[62] M. Shamsi, M. Dehghan, Determination of a control function in three-dimensional parabolic equations by Legendre pseudospectral method, Numer. Methods Partial Differential Equations 28 (2012) 74–93.
[63] R. Baltensperger, M.R. Trummer, Spectral differencing with a twist, SIAM J. Sci. Comput. 24 (2003) 1465–1487.
[64] B.D. Welfert, Generation of pseudo-spectral differentiation, SIAM J. Numer. Anal. 34 (1997) 1640–1657.